Journal of Materials Chemistry C

Accepted Manuscript

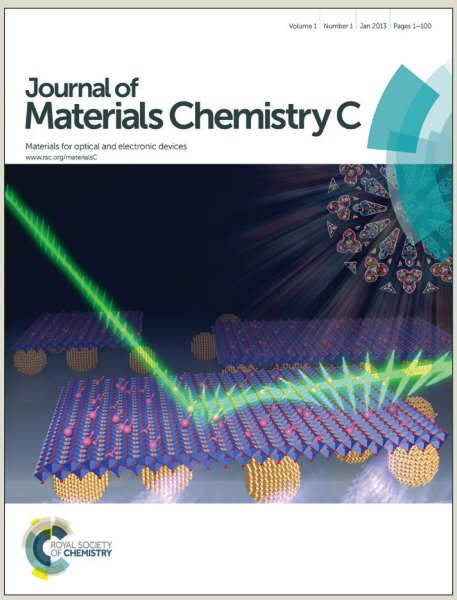

ROYAL SOCIETY OF CHEMISTRY

www.rsc.org/materialsC

Journal Name

RSCPublishing

ARTICLE

Connecting Molecule Oxidation to Single Crystal Structural and Charge Transport Properties in Rubrene Derivatives

Cite this: DOI: 10.1039/xoxxoooooox

Received xxth December 2013,
Accepted xxth January 2014

DOI: 10.1039/xoxxoooooox

www.rsc.org/

S. Uttiya,[a] L. Miozzo, [a] E.M. Fumagalli, [a] S. Bergantin, [a] R. Ruffo, [a] M. Parravicini, [a] A. Papagni, [a] M. Moret, [a] and A. Sassella [a]*

The study of a series of rubrene derivatives properly designed for limiting oxidation can be a powerful tool for clarifying the role of oxidation on the transport properties of crystalline rubrene, still unclear. Here, the synthesis of a series of substituted rubrene derivatives from dimerisation of propargyl alcohols is described together with the analysis of their stability to oxidation and electrochemical properties in solution. Millimetre-sized single crystals of all derivatives are grown and their structure determined from single crystal X-ray diffraction, which shows for all of them crystal packing features closely resembling those of orthorhombic rubrene. Finally, charge transport is studied by means of conductive AFM. The comparison between charge conduction in the crystalline state, oxidation potentials, and photo-oxidation kinetics allows ruling out rubrene endoperoxide as the origin of the high charge conductivity in both rubrene and rubrene derivatives, in agreement with an oxygen-enhanced conductivity model.

Journal Name RSCPublishing

ARTICLE

Introduction

Rubrene (5,6,11,12-Tetraphenyltetracene) is one of the most studied molecular organic semiconductors, since the discovery, a few years ago, of very high charge mobility in rubrene single crystals.[1-4] Rubrene is today the benchmark in single-crystal transistor research, because of its ready availability, its outstanding values of charge mobility, and the ease of crystal growth.[5] Rubrene also presents some advantages over other widespread organic molecular semiconductors, as pentacene and tetracene, since it is significantly more stable, thanks to the aryl substituents on the acene rings, which avoid dimerisation and the formation of tetracene-quinones.

At the same time, the introduction of rubrene into real electronic devices is hindered by some limits, such as its tendency to give a stable endoperoxide and the difficulties found in growing crystalline thin films with the same exciting features observed in single crystals, even though some examples have been presented.[6-15] The origin of some of rubrene interesting properties, such as the high charge conductivity, photoconductivity, and mobility, are not completely understood, in spite of the efforts devoted to find their microscopic origin.

Today it is clear that oxygen plays a key role, because conductivity and photoconductivity of rubrene are increased on exposure to oxygen[16] and diminished by annealing in vacuum.[17] Oxygen-related species probably act as dopants of rubrene but how oxygen-induced defects could affect the electric properties is still unclear and even the chemical nature of these oxygen-induced defects is not completely ascertained. For the chemical origin of oxygen-related band gap states two different hypotheses were proposed, such as (i) the presence of interstitial oxygen molecules or (ii) the formation of rubrene peroxide molecules. According to (i) the enhanced rubrene photoconductivity is the result of a photo-induced electron transfer between molecular oxygen and excited rubrene molecules.[18] According to (ii), rubrene peroxide would produce a localized acceptor state within the band-gap of crystalline rubrene,[19] as deduced from photoluminescence spectroscopy at room temperature[20] and X-ray absorption spectroscopies.[21]

Starting from this background and aiming at the potential use of rubrene in organic electronics, rubrene derivatives bearing different substituents have been recently studied to get some insights on the role of substituents,[22-26] in particular on the electronic properties and on exciton diffusion length in solid state rubrenes.

As for many other intrinsic properties in crystalline organic semiconductors, electrical transport in crystalline rubrene is strongly anisotropic. A monoclinic, a triclinic and an orthorhombic polymorph of rubrene have been described, the latter being the most interesting for applications.[27,28] Charge carriers mobilities as high as 40 cm^2/Vs were indeed measured in orthorhombic rubrene single crystals together with record values for photocurrent generation efficiency and exciton diffusion length.[29,30] In this phase, the molecules are arranged in a herringbone motif, with an efficient $\pi - \pi$ stacking along the *b* axis direction; the largest mobility values have been measured along the *b* axis, so that conduction can be considered to originate from the efficient overlap between molecular π orbitals of neighbouring molecules along the $\pi - \pi$ stacking, as confirmed by pressure dependence of charge carrier transport[31,32] and also demonstrated for similar derivatives.[33] Also the perfect alignment along the short molecular axis between adjacent rubrene molecules plays a key role[34,35] in the triclinic polymorph of rubrene,[28] a small displacement of the molecules along the short axis results in a poor charge carrier mobility.[36]

The peripheral phenyl-phenyl repulsion, which results in a strain in the tetracene core, is one of the factors at the basis of the observed rubrene tendency to react with oxygen. In principle, two approaches can be followed in order to reduce such repulsion: the introduction of electron withdrawing substituents on two of these phenyl rings, which induces their efficient π-π stacking, or the reduction of the steric hindrance of the side groups by replacing phenyl rings with the smaller thienyl rings.

Here, following both approaches, we describe the synthesis of new rubrene derivatives and characterize them, focusing at first on the effects of substituents on the stability to photo-oxidation of the different molecules in solution and on its relationship with oxidation potential and HOMO energy level. Then, single crystals of all the new compounds are grown and their structural characterization addressed, getting full demonstration of a favourable crystal packing, close to that of orthorhombic rubrene. Finally, charge transport measurements are performed on all single crystals: the results fully assess one of the new rubrene derivatives as an organic semiconductor joining transport properties close to those of rubrene with a much higher stability to oxidation. This result definitely supports an oxygen-related process for charge transport enhancement in rubrene, as opposite to a direct role of the product of rubrene oxidation.

Results and Discussion

Synthesis

The interest about rubrene promoted a huge effort to synthesize, functionalize, and characterize derivatives of rubrene.[22-24,33,37-42] The most straightforward synthesis is based on simple heating of 1,1,3-triaryl-3-chloro-allene (1,1,3-triaryl-3-chloro-propan-1,2-diene), as described for the first time in the 1920's and rationalized in the 1970's by Rigaudy.[43] This method is still used for the synthesis of commercial rubrene and has been recently applied to the synthesis of some new derivatives of rubrene.[39,44,45] Due to the reduced number of synthetic steps required by this approach and its compatibility with a wide range of substituents, we selected it to prepare new derivatives of rubrene, bearing electron-withdrawing substituents.

This first step of the synthesis of rubrene according to the allene protocol is the synthesis of appropriate triaryl-propargyl alcohols (Scheme 1). Triaryl-propargyl alcohols can be alternatively prepared by addition of a proper organometallic reagent (e.g. a Grignard reagent of a arylacetylide or a lithium acetylide) to diarylketones (such as benzophenone)[46] or by Sonogashira reaction between a 1,1-diaryl-propargyl alcohol and a halogenated aromatic compound, according to a copper-free protocol already applied to the synthesis of 1,1,3-triaryl propargyl alcohols.[39] A series of derivatives bearing some electron-withdrawing substituents (**1a-c**) was prepared in satisfactory to good yields following the Sonogashira protocol. In order to compare these derivatives with another one bearing an electron-donating moiety, we also prepared a propargyl alcohol (**1d**) bearing a thiophene ring. Alcohol **1d** was prepared following both the above protocols.

For the conversion of these alcohols into rubrene derivatives, we applied the one-pot protocol already described in the literature.[39] Propargyl alcohols **1a-c** were first reacted in 1,1,2,2-tetrachloroethane with mesyl chloride, in the presence of triethylamine, to transform the alcohol into the corresponding chloro-allene. Then, the chloro-allene solutions were heated to reflux in order to convert theses intermediate into the desired

tetraaryltetracenes **2a-c** (Scheme 2). In the case of alcohol bearing a thienyl (**1d**), we developed a new protocol aimed at minimizing competing side reactions leading to the formation of by-products (mainly a 1,3,3-triarylprop-2-en-1-one).

SCHEME 1. Synthesis of propargyl alcohols

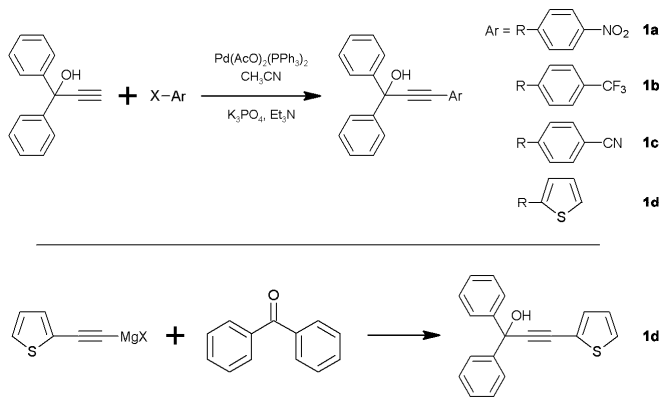

As already reported in the literature,[39,44,45,47,48] the formation of rubrene by dimerisation of triphenyl-chloroallene is always in competition with the formation of a bis-alkylidenecyclobutene. We did not attempt to quantify the amount of this cyclobutene in each reaction, but it was removed quite easily by crystallization from MeOH (see Supplementary Information). During purification of compound **2d**, we obtained several single crystals with different colours and habits, obtained from slow evaporation of a hexane/ethyl acetate 9:1 solution. Single crystal X-ray diffraction data collection performed on these samples revealed, in addition to the formation of cyclobutene, the formation also of a number of unexpected additional side-products. (see Supplementary Information). High purity samples of all tetraaryltetracenes were finally obtained by sublimation under vacuum (6.0×10^{-4} mbar). All the reagents and the compounds were characterized by ^{1}H-NMR, MS, IR and UV-Visible spectroscopy.

SCHEME 2. Synthesis of 5,6,11,12-tetraaryltetracenes

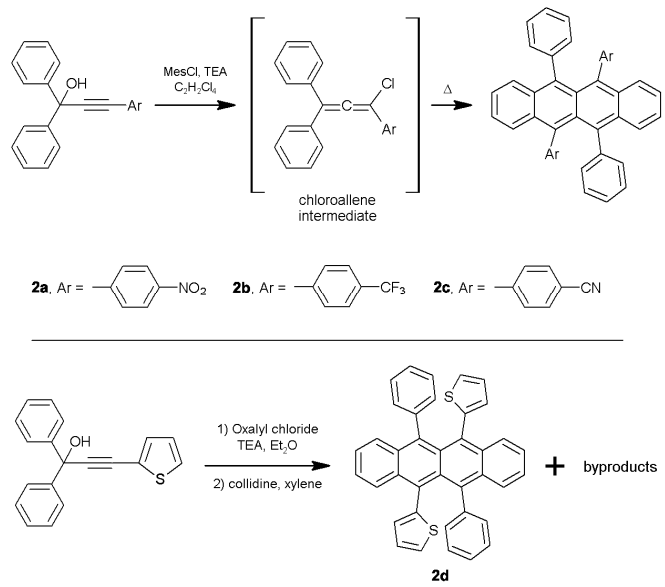

Studies of the new compounds in Solution

Photo-oxidation Kinetics

Rubrene peroxide formation (Scheme 3) is a notable example of reversible photo-peroxidation.[49,50] In general, singlet oxygen ($^{1}O_2$) is responsible for the formation of photoperoxides of many polycyclic aromatic hydrocarbons. The first observation of photo-oxidation of rubrene to its peroxide[51,52] and of its dissociation upon heating or by exposure to light[53] are as old as rubrene itself.

It is well known that the reactivity with $^{1}O_2$ of aromatic hydrocarbons depends on the structure of the $^{1}O_2$ acceptor.[49] In general the reactivity of singlet oxygen with aromatic compounds increases with the electron density of the substrate reflecting the electrophilic nature of $^{1}O_2$. Strain of the aromatic nucleus plays also an important role in the reactivity towards $^{1}O_2$, modifying both the reactivity and the regioselectivity of the reaction. In order to analyze the effect of different substituents on the oxidation rate of rubrene, we performed an analysis of photo-oxidation of rubrene and its derivatives in solution. We prepared solutions of all the rubrene derivatives described above using 1,1,2,2 tetrachloro-ethane as solvent, in two different concentrations (2.2×10^{-4} and 3×10^{-5} M) in order to collect reliable optical absorption spectra in the whole spectral range from 2.1 to 4.5 eV.

SCHEME 3. Photo-oxidation of rubrene leading to rubrene peroxide

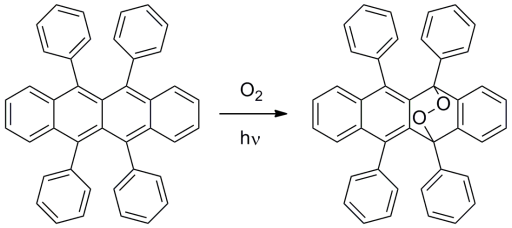

Figure 1 shows the evolution of absorption spectra of (a) rubrene and (b) **2a** solutions with the typical rubrene peaks at 2.3, 2.5, and 2.7 eV. After solution exposure to light and air, we have found the decrease of absorption intensity of these peaks, while a broad band from about 2.8 to 3.6 eV attributed to oxidized rubrene[54,55] grows up, as a function of exposure time (dashed, dotted, and dash-dotted lines). This phenomenon is the result of photo-oxidation in solution, which can therefore be monitored, as discussed in a previous work.[56] Similar spectra were also recorded and monitored for all the other derivatives.

The analysis of the absorption decrease for all compounds has been quantified as the area of the main composite band in the spectra similar as those in Figure 1, integrated from 2.1 to 2.8 eV, as a function of exposure time. In Figure 2 such results are reported for all the compounds and compared to the corresponding rubrene data. The reference value 100% represents the initial integral area, collected immediately after preparation of the solutions. The experiment was performed till the percentage of relative integral area for all molecules decreases to zero, i.e. during a 10 h interval. The same procedure has been applied to the high energy spectral region, using low concentration solutions, by integrating the spectra from 3.6 up to 4.5 eV; the same behaviour is clearly observed (not shown here).

Looking at Figure 2, after the first 20 min exposure to light and air, the integral area of rubrene solution rapidly decreases from 100% to 4%, while for the other solutions it decreases more slowly; for example, the integral area reaches the same value 4% after 45 min and 7.5 h exposure time for the solutions of **2c** and **2a** molecules, respectively. While the rubrene solution becomes transparent in less than 1 h, for all the other compounds full degradation takes from 2 to 10 h, clearly demonstrating the stabilizing effect of the substituents. The highest stabilization is observed in the case of **2a**, according to the strong electron-withdrawing character of 4-nitrophenyl groups.

In our experimental conditions, O_2 concentration is constant and the backwards reaction (from rubrene peroxide to rubrene) can be neglected. Under these hypotheses, we assumed pseudo-first order kinetics for the reaction of rubrene peroxide

formation. This assumption originates from the observed exponential decay of all curves in Figure 2, at least until the integral area goes below 30%, i.e. for most of the process. For longer times, the quantity of unreacted rubrene becomes too low and probably other degradation phenomena become competitive. Down to this 30% area limit, the experimental curves can be accurately fitted by a simple exponential decay of the area A(t):

$$A(t) = A_0 \exp(-kt) \quad (1)$$

where A_0 is the area of the solution spectrum for t = 0 s. In Table 1, second column, we report the values of the oxidation rate *k* extracted from the curves in Figure 2 in time intervals where oxidation obeys the simple rate equation (1).

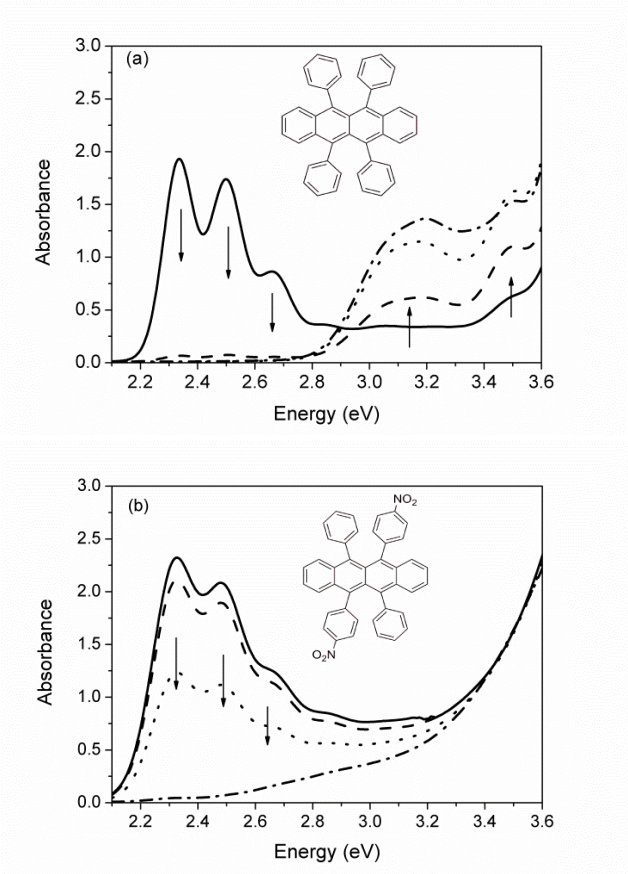

Figure 1. Absorption spectra of (a) rubrene and (b) **2a** solutions, with concentration of 2.2×10^{-4} M, in 10 mm thick quartz cuvette. The spectra were collected immediately after preparation (continuous line), after 20 min (dashed line), after 2h (dotted lines) and after 6h (dash-dotted line) of exposure time under light in air. Inset: molecular structures of (a) rubrene and (b) **2a**.

The introduction of electron withdrawing groups decreases the reactivity of rubrene against $^1O_2$, as expected from standard reactivity of aromatic compounds against electrophiles. The common trend usually observed in the reactivity of organic compounds is respected for all compounds bearing electron-withdrawing groups (**2a-c**). The behaviour of derivative **2d** needs a specific comment. Considering the π-electron-releasing properties of thiophene, a comparable or even higher reactivity against $^1O_2$ than that of rubrene is expected; nonetheless, the experimental data clearly show a degradation rate of **2d** comparable with that of the most stable compound **2a**; this underlines that no special electronic effects on the tetracene core by the thienyl rings are operating. On the other hand, the reduced size of the thienyl ring in comparison to the phenyl one results in a reduction of steric hindrance with the neighbour phenyl ring which partially contributes in releasing the strain in the tetracene core. The electrochemical behaviour of **2d** (see later) also leads to exclude any electron donating effects of the thiophene.

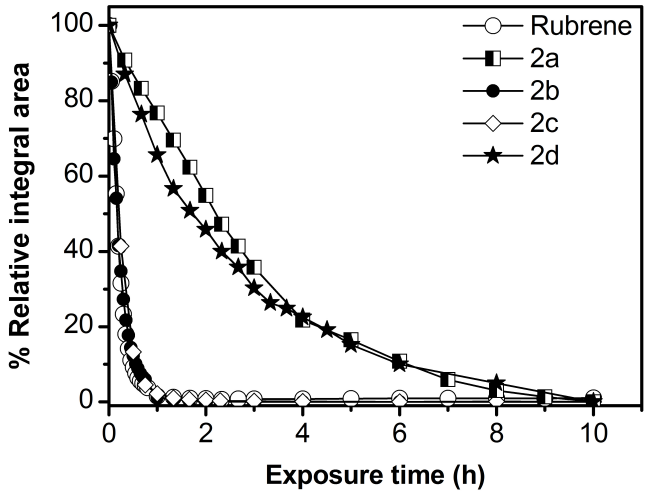

Figure 2. Relative percentage of the area of the absorption band from 2.1 to 2.8 eV of all the solutions as a function of exposure time to light and air.

Table 1. Oxidation rate constant *k*, oxidation potential, and HOMO level of rubrene and all synthesized derivatives **2a-d** in solution.

	Oxidation rate constant *k* (1/h)	Oxidation potential (V)	HOMO level (eV)
rubrene	4.8 ± 0.2	0.40	-5.63
2a	0.36 ± 0.01	0.56	-5.79
2b	4.4 ± 0.1	0.50	-5.73
2c	4.2 ± 0.6	0.53	-5.76
2d	0.39 ± 0.06	0.45	-5.68

Electrochemical Properties

Cyclic voltammetry (CV) and differential pulse voltammetry (DPV) were performed on rubrene and on rubrene derivatives **2a-d** to determine the redox characteristics and HOMO energy levels. Typical CV and DPV anodic curves are shown in Figure 3. Almost all the molecules show a reversible monoelectronic oxidation wave attributed to the formation of the radical cation on the central tetracene core. The redox reaction is not fully reversible only in the case of the thiophene substituted derivative, for this reason all the oxidation potentials have been obtained by DPV. These values are in full agreement with the $E_{1/2}$ calculated from the reversible CV traces observed for the other derivates. Moreover, the rubrene oxidation potential is in agreement with previously reported values in similar electrolyte solution.[57] The nitro, trifluoromethyl, and nitrile derivatives (**2a, 2b, 2c**) display oxidation potentials higher than the rubrene itself, due to the electron withdrawing power of the functional group. The thiophene derivative **2d** has also an oxidation potential slightly higher than the pristine rubrene, despite the donor character of the electron rich heteroaromatic ring. To understand this behaviour we could consider that both rubrene and thiophene are good donor systems and an internal charge transfer process can not be excluded in solution. In this case, the thiophene molecular orbitals contribute to the molecular HOMO orbital and the corresponding oxidation potential is increased to an intermediate value between the oxidation potentials of rubrene and thiophene itself, around 1.2 V vs. ferrocene (Fc). The oxidation potential obtained from the DPV current peak position and the HOMO values

calculated by using a vacuum level of 5.23 V for the Fc/Fc^+ redox couple[58] are listed in Table 1, third and fourth columns.

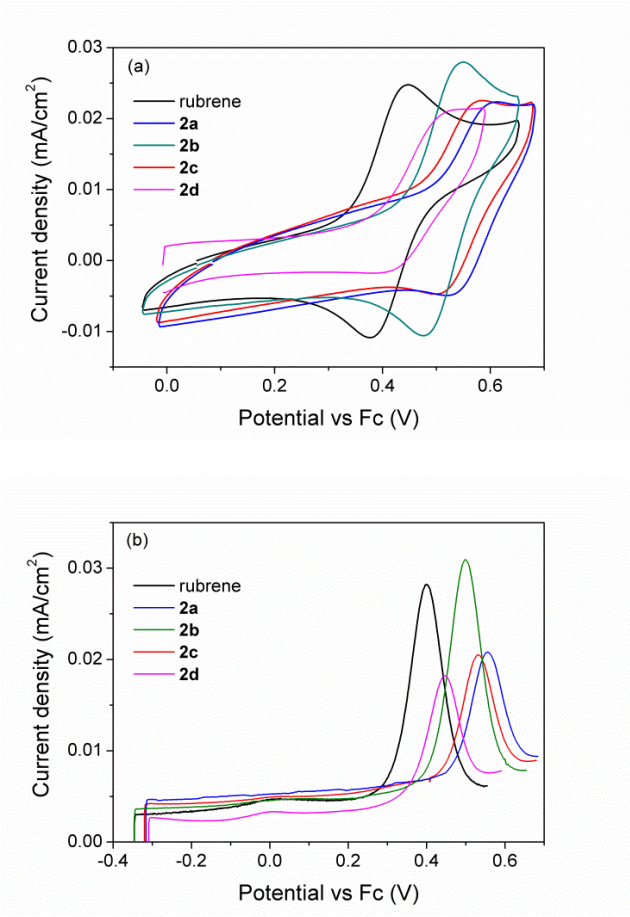

Figure 3. CV traces (a) and PV curves (b) of the different derivatives in 0.1 M $TBAClO_4$ in 2:1 dichloromethane:acetonitrile solution.

The comparison between the data of electrochemical characterization and of photo-oxidation kinetics shows a good agreement, confirming that the introduction of electron-withdrawing substituents (**2a, 2b, 2c**) increases the oxidation potential and decreases the reactivity in the photo-oxidation reaction. Compound **2d** has also an oxidation potential higher than rubrene despite the donor character of the electron rich heteroaromatic ring, but it is worthy to note that derivative **2d** shows a photo-oxidation reactivity similar to **2a** while it has an oxidation potential close to rubrene.

Studies of single crystals of the new compounds

Crystal Structure

All rubrene derivatives **2a-d** display the same crystallographic symmetry adopting the space group $P2_1/c$, so that all individual structural parameters can be easily compared. The most important feature of their crystal structure is the herringbone disposition of the molecules in the (100) layer, involving the long axis of the tetracene: the aromatic cores of adjacent molecules are facing each other π-stacking along the *b* direction of the monoclinic cell, with no short axis displacement. This packing motif is identical to the one found in the (200) layer of orthorhombic rubrene, fully preserved (Figure 4). The different chemical modifications introduced on 4-position of two of the phenyl groups in the rubrene molecule, indeed, allow confinement of the substituents at both surfaces of the (100) layer,[59] leaving almost unaltered the favourable π – π in-plane intermolecular contacts.[34]

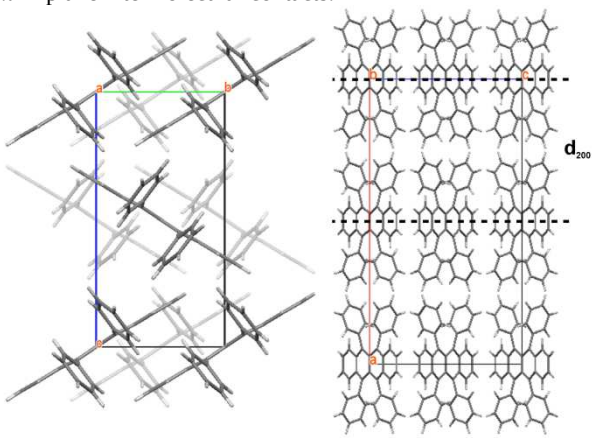

Figure 4. Packing motif of orthorhombic rubrene: [100] view on the left and [010] view on the right.

Analysis of inter- and intra-molecular parameters of compounds **2a-d** (see Table 2) evidences that the packing features closely resemble those of orthorhombic rubrene (considering the data set closest in temperature, CSD code QQQCIG05). In the orthorhombic structure of rubrene, the π–π stacking distance among the tetracene cores of adjacent molecules is 3.67 Å, with a herringbone angle of 61.49°. For all our derivatives, both the π–π stacking distance and the width of the herringbone angle are slightly smaller than in rubrene. While in rubrene the herringbone layer is d_{200} and corresponds to half the *a* cell parameter, with a thickness of 13.39 Å (Figure 4), the elementary layer for the monoclinic structures of all derivatives is d_{100}. The thickness of d_{100} changes with the nature of the substituents since it must accommodate the protruding moieties, sandwiching them between two adjacent layers: derivative **2d** displays the smallest value for d_{100}, even smaller than in rubrene, owing to the absence of substituents on the thienyl rings. On the contrary, to accommodate the bulky trifluoromethyl substituent of derivative **2b**, the widest separation of adjacent layers in the series is observed (Figure 5).

Also the monoclinic β angle is affected by the nature of the substituents, since β is determined by the shift occurring along the *c* axis, which is necessary for the stacking of adjacent d_{100} layers (Figure 6); in orthorhombic rubrene such a shift occurs along the *b* axis and corresponds to half the unit cell parameter. The length of the *b* and *c* axes of our derivatives are, instead, much more similar to each other and to those of orthorhombic rubrene. Moreover, the introduction of the different functionalities does not seem to affect the planarity of the tetracene cores (see Table 2), comparable to that of rubrene. This is expected since the tight herringbone packing is quite demanding in terms of close contacts between adjacent tetracene cores.

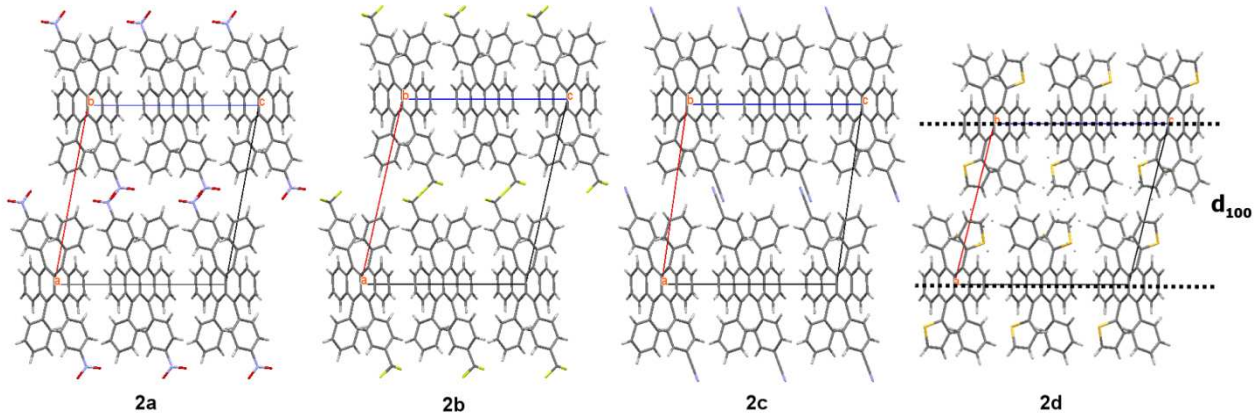

Figure 5. Packing motif of tetraaryltetracenes viewed along [010].

Table 2. Comparison between the structural parameters of rubrene and of derivatives **2a-d**

Compound	**rubrene**	**2a**	**2b**	**2c**	**2d**
Empirical Formula	$C_{42}H_{28}$	$C_{42}H_{26}N_2O_4$	$C_{44}H_{26}F_6$	$C_{44}H_{26}N_2$	$C_{38}H_{24}S_2$
Molecular Weight [g/mol]	532.7	622.65	668.65	582.67	544.71
Crystal System	Orthorhombic	Monoclinic	Monoclinic	Monoclinic	Monoclinic
Space Group	Cmca	$P2_1/c$	$P2_1/c$	$P2_1/c$	$P2_1/c$
Temperature of data collection [K]	125	150	120	120	120
Z / Z'	4/0.25	2/0.5	2/0.5	2/0.5	2/0.5
a [Å]	26.7890(4)	15.0983(3)	15.9782(2)	14.9125(6)	13.5689(5)
b [Å]	7.1730(10)	7.1706(2)	7.2762(6)	7.1151(2)	7.0143(2)
c [Å]	14.246(2)	14.2489(5)	13.9814(6)	14.4263(4)	14.3020(7)
β [°]	-	100.616(1)	102.701(2)	98.099(2)	103.954(2)
V [$Å^3$]	2737.48	1516.24(1)	1585.7(1)	1515.42(9)	1320.94(9)
R_{int}	-	0.0759	0.0505	0.1059	0.0890
R [I > 2σ(I)]	-	0.0673	0.0659	0.0655	0.0687
d_{100} thickness [Å]	13.39	14.84	15.59	14.76	13.17
$d_{\pi\text{-}\pi}$ stacking [Å]	3.67	3.58	3.53	3.63	3.53
Herringbone angle [°]	61.49	59.97(2)	58.04(1)	61.35(1)	60.46(2)
Planarity RMS[a)]	0.033(2)	0.036(2)	0.036(2)	0.034(2)	0.034(2)

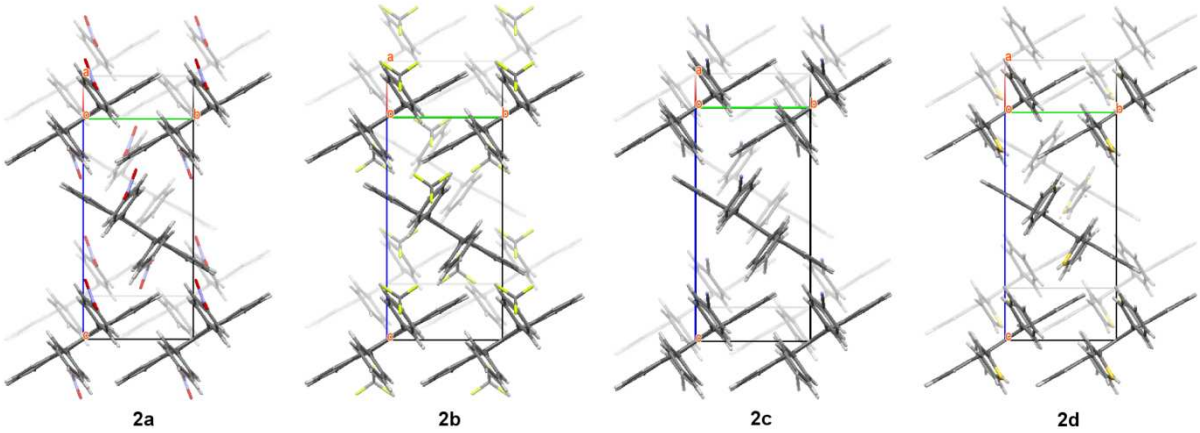

Figure 6. Packing motif of tetraaryltetracenes viewed perpendicularly to (100) plane.

Transport properties

The study of the charge transport properties of a series of single crystals grown from the selected rubrene derivatives was carried out by Conductive Atomic Force Microscopy (c-AFM), a technique particularly suited to study transport properties over micrometre sized or smaller crystals. Using the same experimental conditions and measurement geometry for all the samples (see Supporting Information) it is possible to directly compare the results for different samples.[60,61] Nonetheless, reliable absolute values for mobility

cannot be extracted from c-AFM measurements, due to the incomplete control of geometry of the contacts and to the uncertainty in the determination of the actual tip-sample contact area.[62]

I-V curves in the range ±10 V have been collected in air by measuring the current flowing along the *b* lattice direction, i.e. the direction in which the molecular packing is the same for all the studied rubrene derivatives as well as for rubrene, between the Pt AFM tip and a second electrode, fabricated by a colloidal graphite dispersion. The results for single crystals of rubrene and of compounds **2a**, **2b**, **2c** and **2d** are shown in Figure 7 (a).

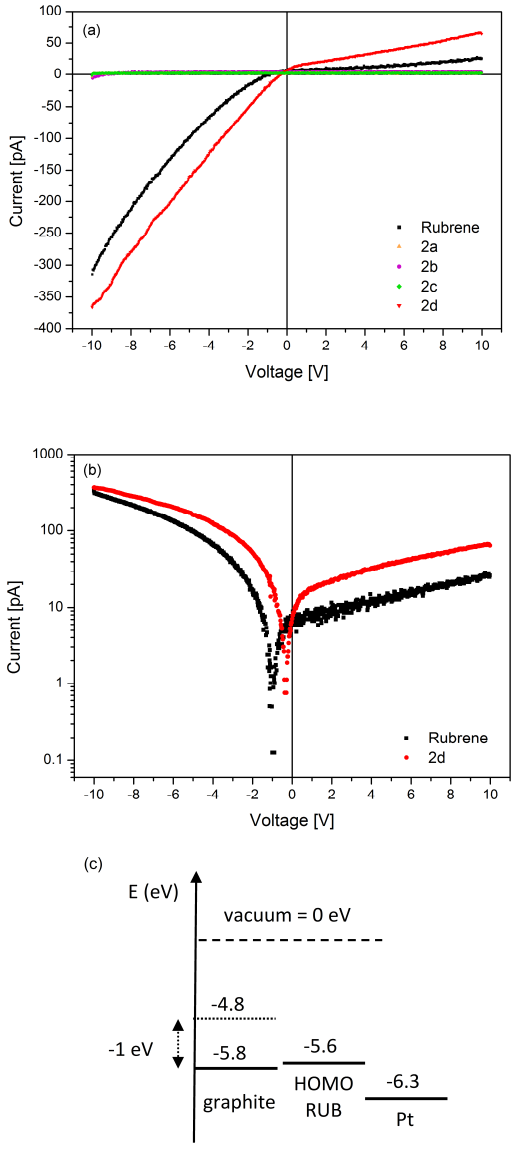

FIGURE 7. I-V curves measured by c-AFM along the *b* axis direction of rubrene and all rubrene derivatives single crystals (a); curves in log scale for rubrene and compound **2d** (b); and sketch of the energy levels for unbiased samples and under -1 V bias (c).

Bias has been applied to the graphite contact, while the AFM tip has been grounded. The I-V curves extracted from **2a**, **2b**, and **2c** are completely flat, indicating that, in the explored bias range, no measurable current can be detected. On the other hand, non-zero current can be measured in the case of rubrene and of derivative **2d** (see also Figure 7 (b)). These two curves are asymmetric, owing to the asymmetry between the two contacts and to the unipolar nature of rubrene and of **2d**. In particular, the larger currents measured for negative bias indicate that the Pt tip is injecting holes into the semiconducting crystals. A sketch of the energy levels involved during c-AFM measurements is reported in Fig. 7 (c) for an applied bias of -1 V, which makes the Fermi levels of the two electrodes align one to another and charge transport occur through the crystal. Even if bulk Pt and graphite levels differ by 1.5 eV, different energy levels should be expected for the Pt-coated tip and the graphite dispersion, used here as electrodes, with respect to bulk materials, so that 1 V bias is enough. Indeed, looking at Figure 7 (b), the I-V curves for rubrene and compound **2d** show the current onset at about -1 V bias, in good agreement with the above sketch.

In the case of rubrene and of its derivative **2d**, maximum current values larger than 300 pA have been measured at -10V bias voltage, indicating that these two materials possess similar transport properties, with larger conductivity than the other derivatives. Being the HOMO level of the different crystals very close, the most relevant result is the oberved conduction and not the HOMO energy of the specific materials.

If experimental data for compounds **2a-c** seem to suggest a positive relationship between slow endoperoxide formation and poor charge conductivity, compound **2d** completely contradicts this hypothesis. Indeed, the latter presents a stability against photo-oxidation comparable with the most stable derivative (**2a**), but in the crystalline state the derivative **2d** displays a charge conductivity comparable with rubrene, which is the most prone to photo-oxidation. On the other side, the comparison between oxidation potentials and charge conductivity of rubrene and compounds **2a-d** shows that the charge conductivity, as measured from c-AFM experiments, is large and comparable for the two compounds with the highest HOMO energy, namely rubrene and **2d**.

Conclusions

Substituted rubrene molecules are synthesized with the aim of improving their stability to photo-oxidation and investigated in solution; their photo-oxidation rate is found to be uncorrelated with respect to their oxidation potential and HOMO level energy. Single crystals of the same molecules show the favourable packing of orthorhombic rubrene, while displaying different transport efficiency, independently of the molecular stability. Trying to propose a unique interpretation of all the results, the rubrene endoperoxide formation can be excluded from the candidate mechanisms responsible for charge carrier improvement in rubrene in the presence of oxygen, while some other oxygen-related processes, favouring intermolecular electron transfer, have to be found. Finally, some compounds, in particular the most stable nitro-rubrene (**2a**), seem to be good organic insulators, therefore being extremely promising materials.

Acknowledgements

The authors acknowledge Fondazione Cariplo (grant 2009/2551) for financial support. The authors thank Federico Tosi and Alberto Gregori for their experimental contribution to the synthesis.

Notes and references

[a] Department of Materials Science, University of Milano Bicocca, via Cozzi 55, I-20125 Milan, Italy.

Electronic Supplementary Information (ESI) available: chemical synthesis, electrochemical characterization, X-ray structural characterization, experimental details on c-AFM.

See DOI: 10.1039/b000000x/

1 D. Braga, N. Battaglini, A. Yassar, G. Horowitz, M. Campione, A. Sassella, and A. Borghesi, *Phys. Rev. B 2008*, **77**, 115205.
2 V. Podzorov, E. Menard, A. Borissov, V. Kiryukhin, J.A. Rogers, and M.E. Gershenson, *Phys. Rev. Lett. 2004*, **93**, 086602.
3 R. Zeis, C. Besnard, T. Siegrist, C. Schlockermann, X. Chi, and C. Kloc, *Chem. Mater. 2005*, **18**, 244.
4 M. Yamagishi, J. Takeya, Y. Tominari, Y. Nakazawa, T. Kuroda, S. Ikehata, M. Uno, T. Nishikawa, and T. Kawase, *Appl. Phys. Lett. 2007*, **90**, 182117.
5 C. Du, W. Wang, L. Li, H. Fuchs, and L. Chi, , *Org. Electron. 2013*, doi: 10.1016/j.orgel.2013.06.006.
6 W.-S. Hu, S.-Z. Weng, Y.-T. Tao, H.-J. Liu, and H.-Y. Lee, *Org. Electron. 2008*, **9**, 385.
7 D. Kafer and G. Witte, *Phys. Chem. Chem. Phys. 2005*, **7**, 2850.
8 E. Fumagalli, M. Campione, L. Raimondo, A. Sassella, M. Moret, L. Barba, and G. Arrighetti, *J. Synchrotron Radiat. 2012*, **19**, 682.
9 M. Campione, M. Moret, L. Raimondo, and A. Sassella, *J. Phys. Chem. C 2009*, **113**, 20927.
10 Z. Li, J. Du, Q. Tang, F. Wang, J.-B. Xu, J.C. Yu, and Q. Miao, *Adv. Mater. 2010*, **22**, 3242.
11 X. Qian, T. Wang, and D. Yan, *Org. Electron. 2013*, **14**, 1052.
12 A. Sassella, L. Raimondo, M. Campione, and A. Borghesi, *Adv. Mater. 2013*, **25**, 2804.
13 L. Raimondo, E. Fumagalli, M. Moret, M. Campione, A. Borghesi, and A. Sassella, *J. Phys. Chem. C 2013*, **117**, 13981.
14 A. Saeki, S. Seki, T. Takenobu, Y. Iwasa, and S. Tagawa, *Adv. Mater. 2008*, **20**, 920.
15 C. Reese and Z. Bao, *Adv. Mater. 2007*, **19**, 4535.
16 V. Podzorov, V.M. Pudalov, and M.E. Gershenson, *Appl. Phys. Lett. 2004*, **85**, 6039.
17 W.-Y. So, J.M. Wikberg, D.V. Lang, O. Mitrofanov, C.L. Kloc, T. Siegrist, A.M. Sergent, and A.P. Ramirez, *Solid State Commun. 2007*, **142**, 483.
18 A.J. Maliakal, J.Y.C. Chen, W.-Y. So, S. Jockusch, B. Kim, M.F. Ottaviani, A. Modelli, N.J. Turro, C. Nuckolls, and A.P. Ramirez, *Chem. Mater. 2009*, **21**, 5519.
19 O. Mitrofanov, D.V. Lang, C. Kloc, J.M. Wikberg, T. Siegrist, W.-Y. So, M.A. Sergent, and A.P. Ramirez, *Phys. Rev. Lett. 2006*, **97**, 166601.
20 O. Mitrofanov, C. Kloc, T. Siegrist, D.V. Lang, W.-Y. So, and A.P. Ramirez, *Appl. Phys. Lett. 2007*, **91**, 212106.
21 X. Song, L. Wang, Q. Fan, Y. Wu, H. Wang, C. Liu, N. Liu, J. Zhu, D. Qi, X. Gao, and A.T.S. Wee, *Appl. Phys. Lett. 2010*, **97**, 032106.
22 K.A. McGarry, W. Xie, C. Sutton, C. Risko, Y. Wu, V.G. Young, Jr., J.-L. Brédas, C.D. Frisbie, and C.J. Douglas, *Chem. Mater.*, 2013, DOI: 10.1021/cm400736s.
23 Y. Zhen, W. Hu, X. Zhang, J.K. Sørensen, X. Fu, G. Zhao, J. Liu, L. Jiang, H. Dong, Z. Shuai, H. Geng, and T. Bjømholm, *J. Mater. Chem.* C, 2013, DOI: 10.1039/C3TC31794C
24 T.K. Mullenbach, K.A. McGarry, W.A. Luhman, C.J. Douglas, and R.J. Holmes, *Adv. Mater. 2013*, **25**, 3689.
25 J. Liu, Q. Meng, X. Zhang, X. Lu, P. He, L. Jiang, H. Dong, and W. Hu, *Chem. Commun. 2013*, **49**, 1199.
26 X. Zhang, J.K. Sørensen, X. Fu, Y. Zhen, G. Zhao, L. Jiang, H. Dong, J. Liu, Z. Shuai, H. Jeng, T. Bjømholm, and W. Hu, *J. Mater. Chem. C 2014*, **2**, 884.
27 O.D. Jurchescu, A. Meetsma, and T.T.M. Palstra, *Acta Crystallogr. 2006*, **B62**, 330.
28 L. Huang, Q. Liao, Q. Shi, H. Fu, J. Ma, and J. Yao, *J. Mater. Chem. 2010*, **20**, 159.
29 H. Najafov, B. Lyu, I. Biaggio, and V. Podzorov, *Phys. Rev. B 2008*, **77**, 125202.
30 H. Najafov, B. Lee, Q. Zhou, L.C. Feldman, and V. Podzorov, *Nat. Mater. 2010*, **9**, 938.
31 Rang, Z.; Nathan, M.I.; Ruden, P.P.; Podzorov, V.; Gershenson, M.E.; Newman, C.R.; Frisbie, C.D. *Appl. Phys. Lett.* **2005**, *86*, 123501.
32 Y. Okada, K. Sakai, T. Uemura, Y. Nakazawa, and J. Takeya, *Phys. Rev. B 2011*, **84**, 245308.
33 S. Haas, A.F. Stassen, G. Schuck, K.P. Pernstich, D.J. Gundlach, B. Batlogg, U. Berens, and H.J. Kirner, *Phys. Rev. B 2007*, **76**, 115203.
34 D.A. da Silva Filho, E.G. Kim, and J.-L. Brédas, *Adv. Mater. 2005*, **17**, 1072.
35 A. Troisi, *Adv. Mater. 2007*, **19**, 2000.
36 T. Matsukawa, M. Yoshimura, K. Sasai, M. Uchiyama, M. Yamagishi, Y. Tominari, Y. Takahashi, J. Takeya, Y. Kitaoka, Y. Mori, and T. Sasaki, *J. Cryst. Growth 2010*, **312**, 310.
37 J. E. Anthony, *Chem. Rev. 2006*, **106**, 5028.
38 J. E. Anthony, *Angew. Chem. Int. Ed. 2008*, ***47***, 452.
39 D. Braga, A. Jaafari, L. Miozzo, M. Moret, S. Rizzato, A. Papagni, and A. Yassar, *Eur. J. Org. Chem. 2011*, **2011**, 4160.
40 J.A. Dodge, J.D. Bain, and A.R. Chamberlin, *J. Org. Chem. 1990*, **55**, 4190.
41 A.S. Paraskar, A.R. Reddy, A. Patra, Y.H. Wijsboom, O. Gidron, L.J.W. Shimon, G. Leitus, and M. Bendikov, *Chem. Eur. J. 2008*, **14**, 10639.
42 Hou, Y.; Chi, X.; Wan, X.; Chen, Y. *J. Mol. Struct.* **2008**, *889*, 265.
43 J. Rigaudy and P. Capdevielle, *Tetrahedron 1977*, **33**, 767.
44 E.V. Banide, P. Oulié, P., and M.J. McGlinchey, *Pure & Appl. Chem. 2009*, **81**, 1.
45 E.V. Banide, C. O'Connor, N. Fortune, Y. Ortin, S. Milosevic, H. Muller-Bunz, and M.J. McGlinchey, *Org. Biomol. Chem. 2010*, **8**, 3997.
46 S.P.G.R. Guinot, J.D. Hepworth, and M. Wainwright, *Dyes Pigm. 2000*, **47**, 129.
47 P. Oulié, L. Altes, S. Milosevic, R. Bouteille, H. Mueller-Bunz, and M.J. McGlinchey, *Organometallics 2010*, **29**, 676.
48 C. Kloc, K.J. Tan, M.L. Toh, K.K. Zhang, and Y.P. Xu, *Appl. Phys. A 2009*, **95**, 219.
49 Yu. A. Arbuzov, *Russ. Chem. Rev. 1965*, **34**, 558.
50 J.-M. Aubry, C. Pierlot, J. Rigaudy, and R. Schmidt, *Acc. Chem. Res. 2003*, **36**, 668.
51 C. Moureu, C. Dufraisse, and P.M. Marshall Dean, *Compt. Rend. 1926*, **182**, 1440.
52 C. Moureu, C. Dufraisse, and P.M. Marshall Dean, *Compt. Rend. 1926*, **182**, 1584.
53 C. Moureu, C. Dufraisse, and L. Girard, *Compt. Rend. 1928*, **186**, 1166.
54 M. Kytka, A. Gerlach, F. Schreiber, and J. Kováč, *Appl. Phys. Lett. 2007*, **90**, 131911.
55 F. Anger, R. Scholz, E. Adamski, K. Broch, A. Gerlach, Y. Sakamoto, T. Suzuki, and F. Schreiber, *Appl. Phys. Lett. 2013*, **102**, 13308.
56 S. Uttiya, L. Raimondo, M. Campione, L. Miozzo, A. Yassar, M. Moret, E. Fumagalli, A. Borghesi, and A. Sassella, *Synth. Met. 2012*, **161**, 2603.
57 K. Okumoto, H. Kanno, Y. Hamada, H. Takahashi, and K. Shibata, *J. Appl. Phys. 2006*, **100**, 044507.
58 D. Veldman, S.C. Meskers, and R.A.J. Janssen, *Adv. Funct. Mater. 2009*, **19**, 1939.
59 S. Bergantin and M. Moret, *Cryst. Growth Des. 2012*, **12**, 6035.
60 H.J. Lee and S.-M. Park, *J. Phys. Chem. B 2004*, **108**, 1590.
61 F. Barrière, B. Fabre, E. Hao, Z.M. LeJeune, E. Hwang, J.C. Garno, E.E. Nesterov, and M.G.H. Vicente, *Macromolecules 2009*, **42**, 2981.
62 O.G. Reid, K. Munechika, and D.S. Ginger, *NanoLetters 2008*, **8**, 1602.